Physical properties and superconductivity of skutterudite-related $Yb_3Co_{4.3}Sn_{12.7}$ and $Yb_3Co_4Ge_{13}$

2001 J. Phys.: Condens. Matter 13 7391

(http://iopscience.iop.org/0953-8984/13/33/319)

INSTITUTE OF PHYSICS PUBLISHING JOURNAL OF PHYSICS: CONDENSED MATTER

J. Phys.: Condens. Matter **13** (2001) 7391–7402 PII: S0953-8984(01)23984-8

Physical properties and superconductivity of skutterudite-related $Yb_3Co_{4.3}Sn_{12.7}$ and $Yb_3Co_4Ge_{13}$

Ya Mudryk[1], A Grytsiv[1], P Rogl[1], C Dusek[2], A Galatanu[2], E Idl[2], H Michor[2], E Bauer[2], C Godart[3], D Kaczorowski[4], L Romaka[5] and O Bodak[5]

[1] Institut für Physikalische Chemie der Universität Wien, Währingerstraße 42, A-1090 Wien, Austria
[2] Institut für Experimentalphysik, TU Wien, Wiedner Hauptstrasse 8–10, A-1040 Wien, Austria
[3] Laboratoire de Chimie Metallurgie des Terres Rares, 2–8 rue Henri Dunant, F94320 Thiais, France,
and CNRS, UPR 209, Place A Briand, 92195 Meudon, France
[4] W Trzebiatowski Institute for Low Temperature and Structure Research, Polish Academy of Sciences, P-50-950 Wroclaw, PO Box 1410, Poland
[5] Department of Inorganic Chemistry, Ivan Franko Lviv National University, 79005 Lviv, Kyryla, and Mefodiya-street 6, Ukraine

E-mail: peter.franz.rogl@univie.ac.at

Received 18 April 2001, in final form 16 May 2001
Published 2 August 2001
Online at stacks.iop.org/JPhysCM/13/7391

Abstract

Rietveld analysis was performed for the intermetallics $Yb_3Co_{4.3}Sn_{12.7}$ and $Yb_3Co_4Ge_{13}$ crystallizing with the closely related structure types, $Yb_3Rh_4Sn_{13}$ and $Yb_3Co_4Ge_{13}$. Below $T_c = 3.4$ K $Yb_3Co_{4.3}Sn_{12.7}$ crosses over into a type-II superconducting ground state with $H_{c2}(0) \sim 2.5$ T. $Yb_3Co_4Ge_{13}$ stays in the normal state down to 300 mK. The γ value of 2.3(2) mJ gat^{-1} K^{-2} and the Debye temperature $\Theta_D = 207(5)$ K deduced from the specific heat as well as T_c correspond to that of elementary Sn, thus indicating conventional BCS superconductivity. Hydrostatic pressure applied to $Yb_3Co_{4.3}Sn_{12.7}$ reveals both an overall decrease of the absolute resistivity values, as well as a decrease of T_c, which vanishes for a critical pressure below 10 kbar. The magnetoresistance of both Yb-based compounds is positive at low temperature but does not exceed 8% in fields of 12 T. The Seebeck coefficient has a maximum value of about 18 μV K^{-1} at $T \sim 250$ K. L_{III} and magnetic susceptibility measurements reveal intermediate valence: 2.66(3) and 2.18(3) for $Yb_3Co_4Ge_{13}$ and $Yb_3Co_{4.3}Sn_{12.7}$, respectively.

1. Introduction

$R_3M_4X_{13}$ compounds, where R is a rare earth element, M is a transition metal and X stands for Ge or Sn, have attracted high attention due to the interesting interplay of superconductivity

and magnetic order [1–3]. From this point of view many papers dealt with the crystal structure [4–11]: in a first attempt Espinosa [5] classified ternary stannides $R_3M_4Sn_{13}$ with respect to their various crystal structures as phases I to VII. Whilst the crystal structures of phases I, II and III were evaluated [4, 6–9, 11] as new unique structure types, phase V and its distortion variant VII were described with the Ir_3Sn_7 type [5]. Further studies revealed [3, 4] that the structure of phase IV is in fact identical with that of phase I, which, at present, is known as $Yb_3Rh_4Sn_{13}$ type (see e.g. [4] and [10] and Typix, standardized settings of crystal structures [12]). In some reports one may find the $Pr_3Rh_4Sn_{13}$ type of structure instead, which according to [8] represents a superstructure type. In our work on $Yb_3Co_{4.3}Sn_{12.7}$ we adopt the $Yb_3Rh_4Sn_{13}$ type following the standardized setting as given in Typix [12]. In similar confusion, the crystal structure of $Yb_3Co_4Ge_{13}$ was first described in [10] to be an isotype of the $Yb_3Rh_4Sn_{13}$ structure (listed as $Pr_3Rh_4Sn_{13}$ type in [13]); however, in an independent study [14], it was said to differ slightly due to splitting of the 24k site for Ge atoms into two about half-filled positions.

Superconducting properties of rare-earth rhodium stannides were investigated in detail in a series of reports [1, 2, 8]; for compounds with other transition metals only brief characteristics were summarized in [3], and no detailed description of their properties was presented in the literature. For example, the superconducting transition temperature for $Yb_3Co_4Sn_{13}$ was roughly estimated as ∼2.5 K [3].

Physical properties of ternary compounds $R_3M_4Ge_{13}$, R = rare earth and M = Ru, Os, presented in [15] mainly concern magnetic ordering at low temperatures (1.9–16.0 K). For the ternary germanides formed by Y and Lu superconductivity was observed at very low temperatures (1.4–3.9 K).

With respect to our recent interest in skutterudite-type thermoelectric materials, $Yb_3Co_4X_{13}$ compounds (X = Ge, Sn) caught our attention because of their structural similarity with the filled ternary skutterudite, $LaFe_4P_{12}$ [16, 17]. In principle, as outlined below, one can conceive both skutterudite and $Yb_3Rh_4Sn_{13}$ type as filled derivatives of the parent perovskite structure.

In due course the present paper deals with a crystal structure refinement of the compounds $Yb_3Co_4X_{13}$ (X = Ge, Sn) and with a detailed investigation of their physical properties.

2. Experiment

The alloys were prepared by argon arc-melting metal pieces of 99.9% minimum purity. To ensure alloy homogeneity, germanium (tin) and cobalt were melted first prior to adding the appropriate amount of ytterbium. Weight losses were insignificant. The $Yb_3Co_4Ge_{13}$ samples were annealed in sealed quartz capsules for 10 days at 1073 K, whereas the $Yb_3Co_{4.3}Sn_{12.7}$ sample was annealed for 3 weeks at 773 K. After heat treatment all samples were quenched in cold water.

Lattice parameters were calculated via a least squares routine from x-ray powder Guinier photographs using Si and Ge as calibration standards. Rietveld refinements of the single-phase samples were performed on x-ray Guinier image plate data obtained from a flat powder specimen in transmission mode (range $8^\circ \leqslant 2\theta \leqslant 100^\circ$, step 0.005 in 2θ, Cu Kα1 radiation) employing the *FullProf98* program [18].

Bulk properties (temperature-, field- and pressure-dependent resistivity and temperature-dependent thermal conductivity and thermopower as well as thermodynamic properties like specific heat and magnetic susceptibility) were obtained by a variety of standard techniques. Details are described in [19]. L_{III} x-ray absorption spectra were measured at two fixed temperatures, 300 and 77 K at the French synchrotron radiation facility (LURE) in Orsay using the x-ray beam of the DCI storage ring (working at 1.85 GeV and ∼320 mA) on the

EXAFS D21 station.

3. Results and discussion

3.1. Structural chemistry

The Guinier films of all $Yb_3Co_4Ge_{13}$ samples prepared were completely indexed on the basis of a primitive cubic cell: the lattice parameters of the samples vary slightly from $a = 0.872\,86(5)$ to 0.872 56(5) nm. In some samples additional minor amounts of germanium were observed. Based on the crystallographic data known for the $Y_3Co_4Ge_{13}$ structure type, results of the Rietveld refinement (figure 1) of a practically single phase sample are presented in table 1. The splitting of the 24k atomic site into two very close partially filled atomic positions was clearly observed, yielding a 2% decrease of the R_I-value in comparison with the 'non-split' model of $Yb_3Rh_4Sn_{13}$ [4], reported in [10].

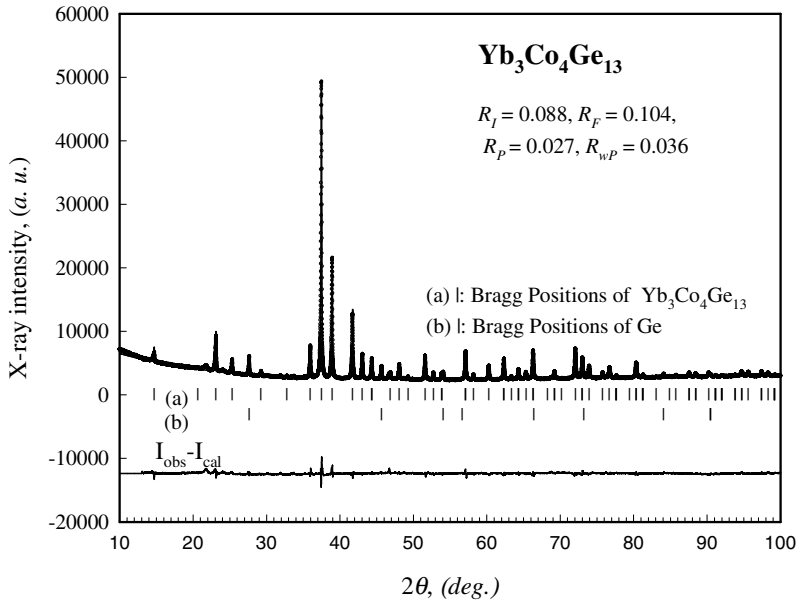

Figure 1. Rietveld refinement of $Yb_3Co_4Ge_{13}$ annealed at 800 °C. The additional minor peaks of Ge are shown. Data collection: Guinier–Huber image plate, Cu Kα_1.

In the case of the $Yb_3Co_{4.3}Sn_{12.7}$ samples synthesized, all Guinier films were completely indexed on the basis of the $Yb_3Rh_4Sn_{13}$ structure type with $a = 0.953\,61(7)$ nm. The sample contains a very small additional amount of tin (figure 2). Results of the structure parameter determination are presented in table 1. Interestingly, a statistical distribution was observed for Co- and Sn-atoms in the 2a sites in contrast to other compounds with the $Yb_3Rh_4Sn_{13}$ structure [4].

Hodeau *et al* [4, 9] have already described the crystal structure of the $R_3M_4Sn_{13}$ compounds (phase I) as a framework of corner-sharing triangular prisms ($RhSn_6$) providing icosahedral, tetracapped rhombic prismatic and cuboctahedral voids, the first and the latter ones filled by Sn(1) and Yb atoms, respectively. The analogy between $R_3M_4Sn_{13}$ compounds and perovskites, $A'A''_3B_4O_{12}$, was emphasized [4, 9], the major difference being the ($RhSn_6$)

Table 1. Structural data (Rietveld refinements) for $Yb_3Co_4Ge_{13}$ and $Yb_3Co_{4.3}Sn_{12.7}$ compounds (data collection: Guinier–Huber image plate; Cu Kα_1; 2θ range: $8 \leqslant 2\theta \leqslant 100$).

Parameter	$Yb_3Co_4Ge_{13}$	$Yb_3Co_{4.3}Sn_{12.7}$
Alloy composition (at.%)	$Yb_{15}Co_{20}Ge_{65}$	$Yb_{15}Co_{20}Sn_{65}$
Structure type	$Y_3Co_4Ge_{13}$	$Yb_3Rh_4Sn_{13}$
Space group	$Pm\bar{3}n$, O_h^3, No 223	$Pm\bar{3}n$, O_h^3, No 223
a (nm)	0.872 86(5)	0.953 61(7)
ρ_x (Mg m^{-3})	8.482	8.750
Reflections measured	76	96
Number of variables	27	24
$R_F = \sum \lvert F_0 - F_c \rvert / \sum F_0$	0.104	0.046
$R_I = \sum \lvert I_{0B} - I_{cB} \rvert / \sum I_{0B}$	0.088	0.049
$R_{wP} = [\sum w_i \lvert y_{0i} - y_{ci} \rvert^2 / \sum w_i \lvert y_{0i} \rvert^2]^{1/2}$	0.036	0.052
$R_P = \sum \lvert y_{0i} - y_{ci} \rvert / \sum \lvert y_{0i} \rvert$	0.027	0.036
$R_e = [(N - P + C)/(\sum w_i y_{0i}^2)]^{1/2}$	0.018	0.021
$\chi^2 = (R_{wP}/R_e)^2$	4.22	6.03
Atom parameters		
Yb	6d ($\frac{1}{4}$ 0 $\frac{1}{2}$)	6d ($\frac{1}{4}$ 0 $\frac{1}{2}$)
B_{iso} (10^2 nm^2)	1.13(2)	1.83(2)
Occ.	1	1
Co	8e ($\frac{1}{4}$ $\frac{1}{4}$ $\frac{1}{4}$)	8e ($\frac{1}{4}$ $\frac{1}{4}$ $\frac{1}{4}$)
B_{iso} (10^2 nm^2)	0.69(4)	1.39(4)
Occ.	1	1
M1	2a (0, 0, 0)	2a (0, 0, 0)
B_{iso} (10^2 nm^2)	0.65(5)	1.80(10)
Occ.	1Ge(1)	0.32Co(1) + 0.68Sn(1)
M2	24k (0 0.1592(3) 0.3271(6))	24k (0 0.157 51(6) 0.304 35(6))
B_{iso} (10^2 nm^2)	1.11(3)	1.80(1)
Occ.	0.59(1) Ge(2)	1Sn(2)
Ge	24k (0 0.1481(4) 0.2800(10))	
B_{iso} (10^2 nm^2)	1.11(3)	
Occ.	0.41(1)	

triangular prisms and the [BO_6] octahedra formed. Following the topological relation of the cubic simple perovskite $CaTiO_3$ and $A'A''_3B_4O_{12}$, obtained by rotation of regular [BO_6] octahedra about the four directions $\langle 111 \rangle$ by about 23° [20], we realize also the close relation to the skutterudite structure $CoAs_3$ [17] with slightly larger rotation of the ($CoAs_6$) octahedra by about 31 to 36° [20]. From the point of view of crystallographic group–subgroup relationships, the structures concerned derive from the parent perovskite type $CaTiO_3$ by doubling of all the unit cell dimensions leading to the $Im\bar{3}m$ subgroup from which two separate branches end up with the cubic primitive $Yb_3Rh_4Sn_{13}$ type and a series of cubic body-centred types with various degrees of filling: WAl_{12}, $CaCu_3Ti_4O_{12}$, $CoAs_3$ and $LaFe_4P_{12}$. Figure 3 portrays the crystallographic relationship resulting in two branches of structure types. It is interesting to note that, as a consequence of the different symmetry and geometrically different (MX_6) units, the 6d site filled by the large Yb atoms in $Yb_3Rh_4Sn_{13}$ corresponds to a much smaller and thus unfilled void in 12e for the body-centred structures with symmetry $Im\bar{3}$. From similar arguments the 6b sites, only filled by copper atoms in $CaCu_3Ti_4O_{12}$, remain unfilled in $Yb_3Rh_4Sn_{13}$.

For convenience table 2 summarizes the atomic positions in the $CoAs_3$ structure type,

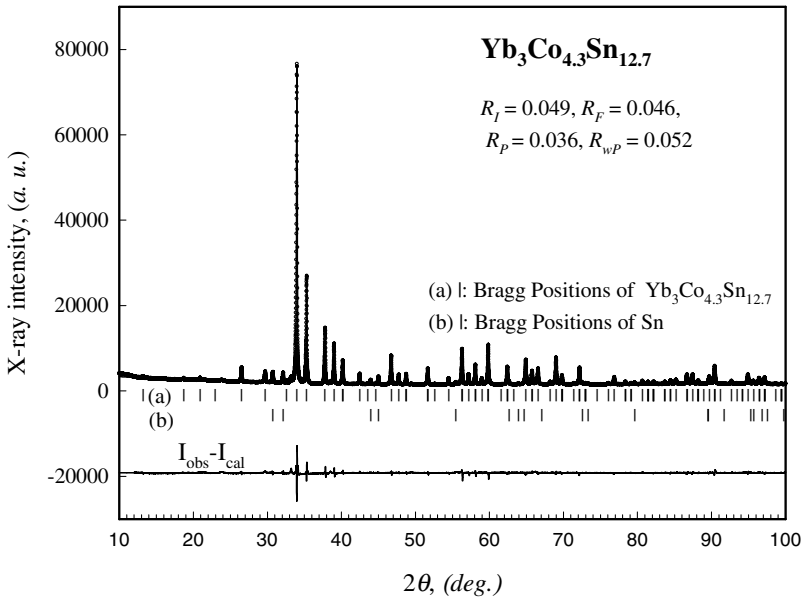

Figure 2. Rietveld refinement of $Yb_3Co_{4.3}Sn_{12.7}$ annealed at 500 °C. The additional minor peaks of Sn are shown. Data collection: Guinier–Huber image plate, Cu Kα_1.

the filled skutterudite $LaFe_4P_{12}$ and the intermetallic $Yb_3Rh_4Sn_{13}$ type revealing the close geometrical relationship.

Table 2. Comparison of the atomic positions in the structure types $CoAs_3$ [17], $LaFe_4P_{12}$ [16] and $Yb_3Rh_4Sn_{13}$ [4] (space group given in brackets).

$CoAs_3$ ($Im\bar{3}$)					$LaFe_4P_{12}$ ($Im\bar{3}$)					$Yb_3Rh_4Sn_{13}$ ($Pm\bar{3}n$)				
Co:	8c	$\frac{1}{4}$	$\frac{1}{4}$	$\frac{1}{4}$	Fe:	8c	$\frac{1}{4}$	$\frac{1}{4}$	$\frac{1}{4}$	Rh:	8e	$\frac{1}{4}$	$\frac{1}{4}$	$\frac{1}{4}$
As:	24g	0	0.1514	0.3442	P:	24g	0	0.1504	0.3539	Sn2:	24k	0	0.150	0.305
					La:	2a	0	0	0	Sn1:	2a	0	0	0
										Yb:	6d	$\frac{1}{4}$	0	$\frac{1}{2}$

From table 2 we clearly see a continuous filling of the interatomic voids in the original skutterudite structure. After filling the 2a sites in both structures, the 6d sites in $Yb_3Rh_4Sn_{13}$ have been filled. The ratio y/z for the 24-fold position, generally very important for skutterudite derivatives, also keeps the same with slight deviations. But, of course, there are some significant differences. First, the inclusion of a new atomic position to the $Yb_3Rh_4Sn_{13}$ structure changes the space group and Bravais symmetry. Furthermore, the rare-earth atoms in $LaFe_4P_{12}$ occupy the 2a position, whilst in $Yb_3Rh_4Sn_{13}$ this position is occupied by smaller Sn atoms (in case of $Yb_3Co_{4.3}Sn_{12.7}$ by a mixture of Co and Sn atoms). The largest atoms (rare earth) in $Yb_3Rh_4Sn_{13}$ are situated in the voids formed by smaller atoms and definitely have changed the coordination polyhedra for transition metal atoms (figure 3) and tin.

It is also clearly seen from table 1 that the $Yb_3Co_4Ge_{13}$ structure type derives from the $Yb_3Rh_4Sn_{13}$ type by splitting the 24k atomic position into two very close partially filled sites. Of course, the coexistence of these two atoms in one void is impossible and they change from one to the other in such a way that the overall occupation of this 24k site is equal to

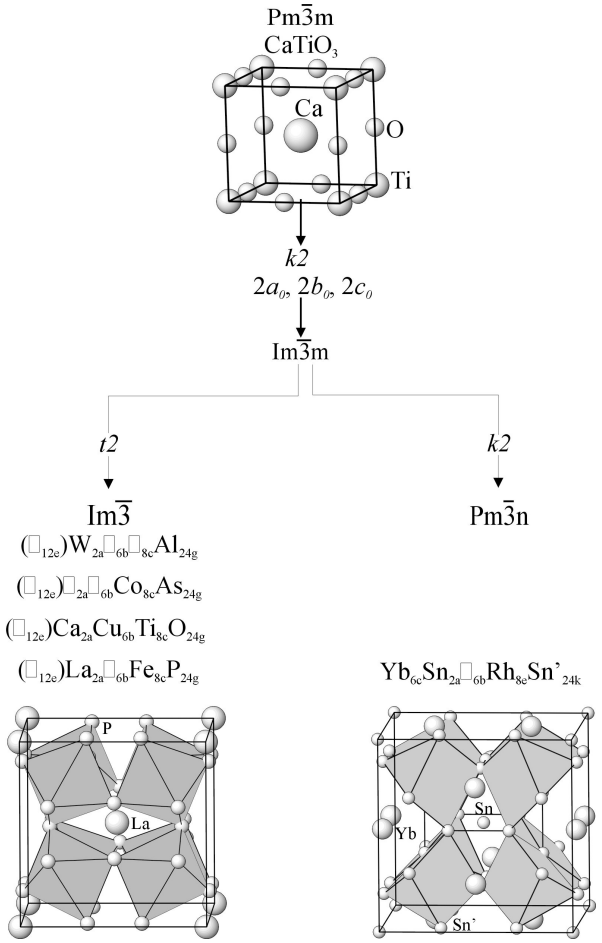

Figure 3. Structure relations between parent $CaTiO_3$ and derivatives. The transition metal atoms M are within the shaded coordination polyhedra.

$$0.59 + 0.41 = 1.$$

3.2. Physical behaviour

3.2.1. The superconducting state of $Yb_3Co_{4.3}Sn_{12.7}$. The temperature-dependent resistivity $\rho(T)$ of $Yb_3Co_4Ge_{13}$ and $Yb_3Co_{4.3}Sn_{12.7}$ is displayed in figure 4 in a normalized representation for temperatures above 4.2 K. The respective room temperature values are 4.40 and 2.70 $\mu\Omega$ m. Both compounds are characterized by a metallic behaviour; however the overall features are different. $Yb_3Co_4Ge_{13}$ can be satisfactorily accounted for in terms of the modified Bloch–Grüneisen law [21]

$$\rho(T) = \rho_0 + 4R\Theta_D\left(\frac{T}{\Theta_D}\right)^5 \int_0^{\Theta_D/T} \frac{x^5\,\mathrm{d}x}{(\mathrm{e}^x - 1)(1 - \mathrm{e}^{-x})} - KT^3 \qquad (1)$$

where R is a temperature-independent electron–phonon interaction constant, Θ_D is the Debye temperature and KT^3 is the Mott–Jones term due to scattering processes of the conduction

electrons on a narrow feature of the density of states in the vicinity of the Fermi energy. A least squares fit of equation (1) to the experimental data reveals $\Theta_D = 350$ K and $R = 0.007\ \mu\Omega$ m K^{-1}. $Yb_3Co_{4.3}Sn_{12.7}$, however, deviates significantly from such a common shape of metallic resistivity curves. Rather, the empirical formula of Woodward and Cody [22]

$$\rho = \rho_0 + \rho_1 T + \rho_2 \, e^{-(T_0/T)} \tag{2}$$

can be used to describe $\rho(T)$ of $Yb_3Co_{4.3}Sn_{12.7}$ from 4.2 K up to room temperature. The characteristic temperature in this case is evaluated as $T_0 = 66$ K. At variance with the Bloch–Grüneisen law, no theoretical justification exists for the above formula, developed in order to trace $\rho(T)$ of Cr_3Si-type and other superconductors. Equation (2) yields a strong curvature at low temperatures and accounts for some tendency towards saturation in the high temperature limit. In fact, as evidenced from our low temperature studies ($T_{min} \sim 0.3$ K), $Yb_3Co_{4.3}Sn_{12.7}$ crosses over into a superconducting ground state below $T_c = 3.4$ K, see figure 5, while $Yb_3Co_4Ge_{13}$ is in the normal state in the covered temperature range. The application of an external magnetic field diminishes T_c and the critical field H_{c_2} is estimated to be about 2.5 T (inset, figure 5). The upper critical field H_{c_2} can be used to estimate the coherence length of the present Yb compound within the weak-coupling theory [23]:

$$\mu_0 H_{c2}(0) = \Phi_0 / 2\pi \zeta_0^2. \tag{3}$$

Here, the flux quantum $\Phi_0 = h/2e = 2.07 \times 10^{-15}$ T m^2; thus, $\zeta \cong 11.5$ nm.

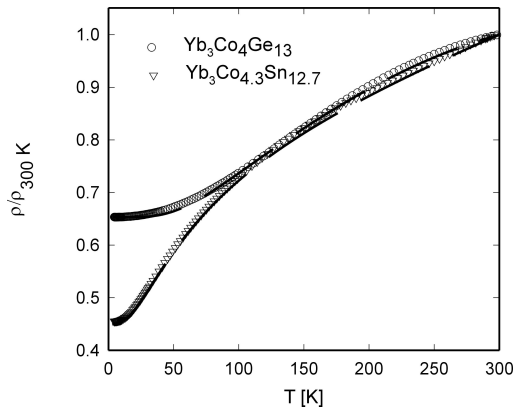

Figure 4. Normalized temperature dependent resistivity ρ of $Yb_3Co_4Ge_{13}$ and $Yb_3Co_{4.3}Sn_{12.7}$. The solid lines are least squares fits (see text).

Basic properties of the superconducting state follow also from heat capacity measurements. Shown in figure 7 is the specific heat C_p of $Yb_3Co_{4.3}Sn_{12.7}$ plotted as C_p/T against T at various values of externally applied magnetic fields. For the purpose of comparison, a.c. susceptibility data are added (right axis). The onset of superconductivity, as derived from $\chi_{a.c.}$, occurs below 3.35 K, in agreement with the above resistivity measurement, while the heat capacity data indicate bulk superconductivity below $T_c = 2.95$ K. However, a small amount of antiferromagnetically ordered Yb_2O_3 modifies the heat capacity in the vicinity of $T_N \sim 2.2$ K. BCS theory in the weak-coupling limit provides a relation between the jump of the specific heat at T_c and the normal state electronic contribution, γ, i.e., $\Delta C_p/(\gamma T_c) = 1.43$. Taking the appropriate numbers as derived from figure 7 reveals a value very near to that of the BCS theory, $\Delta C_p/(\gamma T_c)(\mathrm{exp}) = 1.5(1)$. The proximity of the experimental value to that of the BCS theory allows us furthermore to calculate the thermodynamic critical field $H_c(0)$ as the condensation

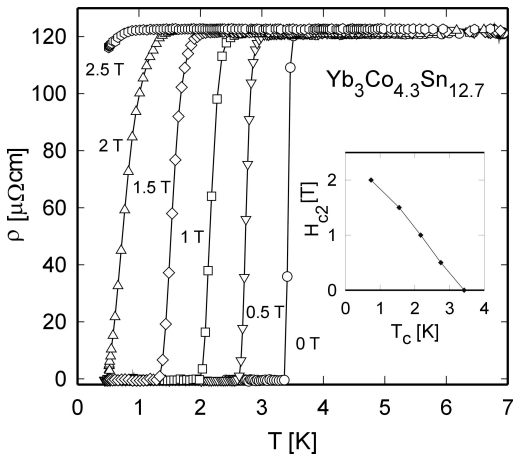

Figure 5. Temperature-dependent resistivity ρ of $Yb_3Co_{4.3}Sn_{12.7}$ measured at various externally applied magnetic fields. The inset shows the critical field H_{c2} as a function of temperature.

energy of the Cooper pairs from specific heat data and subsequently the Ginzburg–Landau parameter κ [23]. The appropriate BCS ratio is given by $\gamma T_c^2/H_c^2(0) = 0.168$. Using $\gamma = 46$ (4) mJ mol^{-1} K^{-2} yields $\mu_0 H_c(0) \sim 30$ mT. The Ginzburg–Landau parameter κ is then derived from $\kappa = \lambda/\zeta = H_{c2}/\sqrt{2}H_c \sim 60$ and finally the London penetration depth $\lambda = 680$ nm. The initial slope of the critical field of $Yb_3Co_{4.3}Sn_{12.7}$, deduced from specific heat (compare figure 7) as well as from resistivity data (compare figure 5), is evaluated as -0.8 T K^{-1}.

The electron–phonon coupling as the driving mechanism to form Cooper pairs can be inferred from the soft lattice of the Yb compound, reflected by a Debye temperature of the order of 200 K ($\Theta_D = 207(5)$ K, taken from $C_p(T)$ data above 4 K). Moreover, the deduced γ value of the specific heat of 46(4) mJ mol^{-1} K^{-2}, equivalent to 2.3(2) mJ gat^{-1} K^{-2} and $\Theta_D = 207(5)$ K is similar to $\gamma = 1.78$ mJ gat^{-1} K^{-2} and $\Theta_D = 195$ K of elementary Sn, respectively. Also the condensation energy $\mu_0 H_c(0) \sim 30$ mT coincides with the value of Sn, $\mu_0 H_c(0) = 30.5$ mT; however, the upper critical field of the former is about 70 times larger. Figure 7 displays a twofold transition into the superconducting state, with $T_{c2} = 3.35$ K and $T_{c1} = 2.95$ K. The former temperature coincides with the transition temperature deduced from the a.c. susceptibility measurement as well as with the resistivity study and indicates therefore a significant volume fraction being superconducting already at T_{c2}.

Another proof of the standard electron–phonon coupling as the mechanism for superconductivity follows from the pressure response of this system. Hydrostatic pressure applied to $Yb_3Co_{4.3}Sn_{12.7}$ reveals both an overall decrease of the absolute resistivity values, as obvious from figure 6, as well as a decrease of T_c, which vanishes for a critical pressure below 10 kbar (inset, figure 6). In order to derive the change of the Debye temperature upon increasing pressure, we have analysed the data below 100 K by the modified Bloch–Grüneisen law, equation (1), which satisfactorily describes the resistivity behaviour in such a limited temperature range. The results of least squares fits to $\rho(T, p)$ evidence an increase of the Debye temperature of about 5% when proceeding from $p = 1$ bar to $p = 15$ kbar. In the context of McMillan's formula, where T_c is related to the Hopfield parameter $\eta = N(E_F)\langle I\rangle$ (with $\langle I\rangle$ the electron–phonon matrix element) and to the Debye temperature Θ_D, an increasing value of Θ_D causes a decrease of T_c. The latter is obvious from the inset in figure 6.

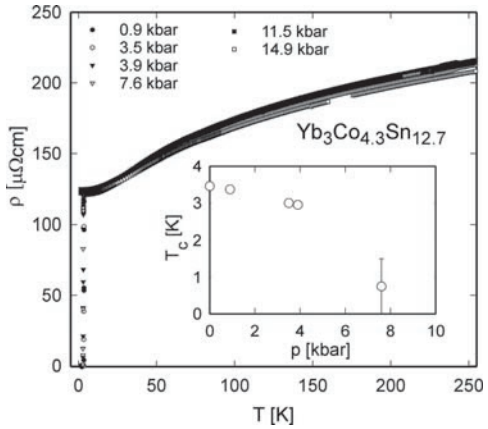

Figure 6. Temperature dependent resistivity ρ of $Yb_3Co_{4.3}Sn_{12.7}$ measured at various values of applied hydrostatic pressure. The inset shows the pressure dependent superconducting transition T_c.

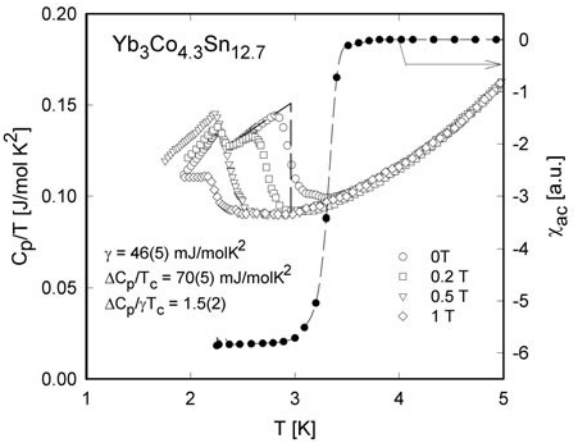

Figure 7. Specific heat C_p of $Yb_3Co_{4.3}Sn_{12.7}$ for various externally applied magnetic fields plotted as C_p/T against T. The dashed line indicates an idealized phase transition. The right axis refers to a.c. susceptibility.

The magnetoresistance of both Yb-based compounds is positive at low temperature but does not exceed 8% in fields of 12 T. The positive sign reveals dominance of the classical magnetoresistance. The Seebeck coefficient of these compounds is larger than that of simple metals, finding its maximum at $T \sim 250$ K with a value of about 18 μV K^{-1}. However, the huge values of thermoelectric power found in many members of the closely related skutterudites have not been observed, excluding these Yb compounds from thermoelectric applications.

3.2.2. Magnetic behaviour of $Yb_3Co_4Ge_{13}$ and $Yb_3Co_{4.3}Sn_{12.7}$. In order to obtain information about the magnetic state of the Yb ions in both compounds, L_{III} and susceptibility measurements were performed. Shown in figure 8 are the energy-dependent L_{III} spectra of $Yb_3Co_4Ge_{13}$ and $Yb_3Co_{4.3}Sn_{12.7}$ at 300 and 77 K, respectively. Both spectra show two features around 8937 and 8943 eV corresponding to Yb being divalent and trivalent, respectively. The

structure at 8937 eV is reinforced in the case of $Yb_3Co_{4.3}Sn_{12.7}$ as compared to $Yb_3Co_4Ge_{13}$, which is due to a higher concentration of the divalent state. We also notice that this structure slightly increases as the temperature is lowered from room temperature down to 77 K, which establishes that the valence is temperature dependent, a characteristic of intermediate valence materials. After subtraction of the background in a standard manner, the edge was decomposed into a pair of Lorentzians and modified inverse tangent functions to provide the relative weight of the two electronic configurations and to evaluate the valence $\nu(L_{III})$ of the Yb-ions. Thus we observed ν-values of 2.66(3) and 2.18(3) at 77 K for $Yb_3Co_4Ge_{13}$ and $Yb_3Co_{4.3}Sn_{12.7}$, respectively. Sommerfeld values of the specific heat, γ, in such compounds exhibit typically some tens of mJ mol^{-1} K^{-2} as in fact was deduced for $Yb_3Co_{4.3}Sn_{12.7}$. Superconductivity for the latter is then associated with an almost divalent Yb ion and not a consequence of heavy fermion state.

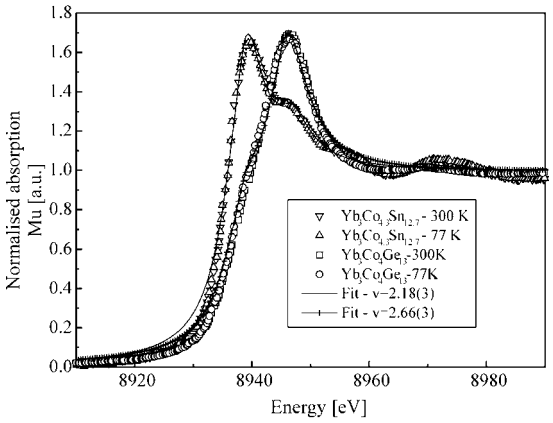

Figure 8. Energy-dependent L_{III} absorption edge spectra of $Yb_3Co_4Ge_{13}$ and $Yb_3Co_{4.3}Sn_{12.7}$ derived at 300 K and 77 K, respectively. The solid lines are least squares fits (see text).

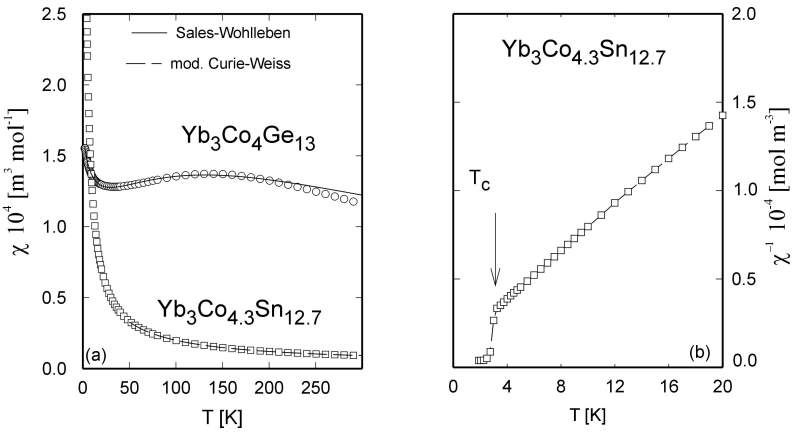

Figure 9. (a) Temperature-dependent magnetic susceptibility χ of $Yb_3Co_4Ge_{13}$ and $Yb_3Co_{4.3}Sn_{12.7}$. The solid and the dashed line represent fits according to the Sales–Wohlleben and the modified Curie–Weiss law, respectively. (b) Temperature-dependent inverse susceptibility χ^{-1} of $Yb_3Co_{4.3}Sn_{12.7}$. The superconducting transition is shown by an arrow.

Intermediate valence of the Yb ions causes also significant deviations of the magnetic susceptibility χ from the standard Curie–Weiss behaviour. As an example, the temperature-dependent $\chi(T)$ of $Yb_3Co_4Ge_{13}$ is displayed in figure 9(a). The observed susceptibility appears to be typical for intermediate valence with spin fluctuation effects. The Sales–Wohlleben model [24]

$$\chi(T) = \frac{N\mu_{eff}^2[1 - v(T)]}{3k_B(T + T_{sf})} \tag{4}$$

where T_{sf} denotes a characteristic temperature associated with fluctuations between the $4f^{13}$ and $4f^{14}$ states and $\mu_{eff} = 4.54\ \mu_B$, satisfactorily describes the experimental $\chi(T)$ data when taking into account magnetic impurities as observed at low temperatures from the rapid rise of $\chi(T)$ at low temperatures. The function $v(T)$ represents the mean occupation of the ground state, which is temperature and energy dependent according to [24]

$$v(T) = \frac{1}{1 + 8\exp[-E_{ex}/k_B(T + T_{sf})]}. \tag{5}$$

A least squares fit reveals the spin-fluctuation temperature $T_{sf} = 226$ K and the exchange energy between $4f^{13}$ and $4f^{14}$ levels $E_{ex} = 770$ K. The valence $v(77\ \text{K}) = 2.61$ is in fine agreement with the value obtained from L_{III} analysis ($v = 2.66$).

The magnetic susceptibility of $Yb_3Co_{4.3}Sn_{12.7}$ was analysed above about 50 K in terms of the modified Curie–Weiss law, i.e., $\chi = \chi_0 + C/(T - \theta_p)$ (dashed line, figure 9(b)), resulting in a rather small magnetic moment $\mu_{eff} = 1.1\ \mu_B$/Yb, $\theta_p \sim -15$ K evidencing antiferromagnetic correlations. Panel (b) of figure 9 shows low temperature features of $Yb_3Co_{4.3}Sn_{12.7}$ where the onset of superconductivity is found from a sudden drop of χ^{-1} below about 3.4 K. Due to the presence of traces of trivalent, magnetic Yb_2O_3, diamagnetism of the superconducting state is superimposed by the paramagnetic oxide contribution.

4. Summary

Intermetallics $Yb_3Co_{4.3}Sn_{12.7}$ and $Yb_3Co_4Ge_{13}$ were studied with respect to thermodynamics, transport properties and x-ray absorption. The structure types were analysed in terms of crystallographic group–subgroup relations to derive from perovskite. With respect to the close correspondence to the skutterudite type of structure, thermoelectric behaviour was investigated; however, the Seebeck coefficients do not exceed a maximum value of about 18 μV K^{-1}, well below useful thermoelectric criteria.

Whilst $Yb_3Co_4Ge_{13}$ stays in the normal state down to 300 mK, $Yb_3Co_{4.3}Sn_{12.7}$ crosses over into a type-II superconducting ground state with $T_c = 3.4$, $H_{c2}(0) \sim 2.5$ T and a Ginzburg–Landau parameter $\kappa \sim 60$. The superconducting parameters and physical features observed are consistent with conventional BCS superconductivity. The Sommerfeld value $\gamma = 2.3$ (2) mJ gat^{-1} K^{-2}, the Debye temperature $\Theta_D = 207(5)$ K, both deduced from the specific heat, and additionally T_c match the corresponding characteristics of elementary Sn. With a lower degree of filling the 4f band in $Yb_3Co_4Ge_{13}$ in respect to almost $4f^{14}$-type $Yb_3Co_{4.3}Sn_{12.7}$ it is plausible that $Yb_3Co_4Ge_{13}$ stays in a normal ground state rather than exhibiting superconductivity.

L_{III} and magnetic susceptibility measurements reveal intermediate valence: 2.66(3) and 2.18(3) for $Yb_3Co_4Ge_{13}$ and $Yb_3Co_{4.3}Sn_{12.7}$, respectively. The intermediate valence nature of the Yb ions and the only slightly enhanced γ value of the specific heat are fingerprints of a normal type of superconductivity, rather than a scenario invoking heavy quasi-particles as found in heavy fermion superconductors.

Acknowledgments

This research was sponsored by the Austrian FWF under grant P12899 and P13778 as well as by a grant for an international joint research project NEDO (Japan). Ya Mudryk is grateful to the OEAD for a four month fellowship in Austria.

References

[1] Shenoy G K, Dunlap B D and Fradin F Y (eds) 1981 *Ternary Superconductors* (Amsterdam: Elsevier–North-Holland) p 219
[2] Remeika J P *et al* 1980 *Solid State Commun.* **34** 923
[3] Espinosa G P, Cooper A S and Barz H 1982 *Mater. Res. Bull.* **17** 963
[4] Hodeau J L, Chenavas J, Marezio M and Remeika J P 1980 *Solid State Commun.* **36** 839
[5] Espinosa G P 1980 *Mater. Res. Bull.* **15** 791
[6] Cooper A S 1980 *Mater. Res. Bull.* **15** 799
[7] Vandenberg J M 1980 *Mater. Res. Bull.* **15** 835
[8] Hodeau J L, Marezio M, Remeika J P and Chen C H 1982 *Solid State Commun.* **42** 97
[9] Hodeau J L, Marezio M and Remeika J P 1984 *Acta Crystallogr.* B **40** 26
[10] Venturini G, Méot-Meyer M, Malaman B and Roques B 1985 *J. Less-Common Met.* **113** 197
[11] Miraglia S, Hodeau J L, Marezio M, Laviron C, Ghedira M and Espinosa G P 1986 *J. Solid State Chem.* **63** 358
[12] Parthe E *et al* 1994 *Typix Standardized Data and Crystal Chemical Characterization of Inorganic Structure Types* 8th edn (Berlin: Springer) 1597
[13] Villars P and Calvert L D (eds) 1991 *Pearson's Handbook of Crystallographic Data for Intermetallic Phases* 2nd edn (Ohio Materials Park: ASM)
[14] Bruskov V A, Pecharskii V K and Bodak O I 1985 *Izv. Akad. Nauk SSSR, Neorg. Mater.* **22** 1289
[15] Segre C U, Braun H F and Yvon K 1981 *Ternary Superconductors* ed G K Shenoy, B D Dunlap and F J Fradin (Amsterdam: Elsevier–North-Holland) 243
[16] Jeitschko W and Braun D 1977 *Acta Crystallogr.* B **33** 3401
[17] Oftedal I 1928 *Z. Kristallogr.* A **66** 517
[18] Rodriguez-Carvajal J 1990 *Abstracts Satellite Meeting on Powder Diffraction XV Congress Int. Union Crystallogr. (Toulouse)*
[19] Bauer E, Galatanu A, Michor H, Hilscher G, Rogl P and Boulet H 2000 *Eur. Phys. J.* B **14** 483
[20] O'Keeffe M and Hyde B G 1977 *Acta Crystallogr.* B **33** 3802
[21] Meaden G T 1971 *Contemp Phys.* **12** 313
[22] Woodward D W and Cody G D 1964 *Phys. Rev.* A **136** 166
[23] Schmidt V V 1977 *The Physics of Superconductors* ed P Müller and A V Ustinov (Berlin: Springer)
[24] Sales B C and Wohlleben D K 1975 *Phys. Rev. Lett.* **35** 1240